Geophysical Research Letters

RESEARCH LETTER
10.1029/2019GL084776

Key Points:
- Pyroclastic density currents, as snow avalanches, are ground-hugging flows formed by collapsing volcanic fountains
- The entrainment rate regulates the amount of surrounding fluid that enters gravity density currents and controls flow mobility
- A power law model is presented for the entrainment rate that can help modeling the flow of hazardous geophysical density currents

Supporting Information:
- Supporting Information S1
- Table S1
- Table S2

Correspondence to:
P. Dellino,
pierfrancesco.dellino@uniba.it

Citation:
Dellino, P., Dioguardi, F., Doronzo, D. M., & Mele, D. (2019). The entrainment rate of non-Boussinesq hazardous geophysical gas-particle flows: An experimental model with application to pyroclastic density currents. *Geophysical Research Letters*, *46*. https://doi.org/10.1029/2019GL084776

Received 11 AUG 2019
Accepted 27 OCT 2019
Accepted article online 19 NOV 2019

The Entrainment Rate of Non-Boussinesq Hazardous Geophysical Gas-Particle Flows: An Experimental Model With Application to Pyroclastic Density Currents

P. Dellino[1], F. Dioguardi[2], D. M. Doronzo[3], and D. Mele[1]

[1]Dipartimento di Scienze della Terra e Geoambientali, Università di Bari, Bari, Italy, [2]British Geological Survey, The Lyell Centre, Edinburgh, UK, [3]Institute of Earth Sciences "Jaume Almera," ICTJA, CSIC, Group of Volcanology, SIMGEO UB-CSIC, Barcelona, Spain

Abstract The entrainment rate of pyroclastic density currents is investigated by large-scale experiments. The ground flows are initiated by the impact on the terrain of a dense gas-particle fountain issuing from a cylindrical conduit, similarly to natural volcanic events. On impact, the excess density with respect to the surrounding atmosphere was up to 11.6 kg/m^3, making the currents non-Boussinesq. A power law model of the entrainment rate is developed, which is similar to that proposed for snow avalanches by Ancey (2004, https://doi.org/10.1029/2003JF000052) and is verified for the Richardson's number range between 0.25 and 5.95. Rapid changes of the entrainment are caused by (i) strong accelerations at the fountain impact on the ground; (ii) break in slope; and (iii) topographic obstacles. Such changes, together with the sedimentation rate, influence flow mobility. The use of the power law is suggested for modeling the motion of unsteady hazardous geophysical mass flows such as pyroclastic density currents and snow avalanches.

Plain Language Summary Pyroclastic density currents form from volcanic fountains and, as other ground-hugging currents, like snow avalanches, incorporate air, and expand along runout. Air entrainment is one of the factors that control the mobility of such huge, devastating currents. In this paper the entrainment rate is simulated by large-scale experiments, which can help modeling the motion of such hazardous geophysical gas-particle flows.

1. Introduction

Pyroclastic density currents are ground-hugging flows that move down the slope of volcanoes and spread for long distance over the surrounding area (Dufek, 2016; Sulpizio et al., 2014). They represent the most devastating phenomena of explosive eruptions and are often initiated by a few-kilometer-high gas-particle fountains issuing at high velocity from a crater. As the fountain impinges on the terrain, the normal stress of the descending flow is transformed into tangential stress, which generates a turbulent shear current, up to hundreds of meters deep, moving laterally. Its speed, in the range of tens of meters per second, is governed by the excess density of the fluid mixture with respect to the surrounding atmosphere. The current is made of a dispersion of gas and dense solid particles with bulk mixture density:

$$\rho_{mix} = \rho_s C + \rho_g (1-C) \quad (1)$$

with ρ_s particle density, C particle volumetric concentration, and ρ_g gas density. Since particle density is in the order of 10^3 kg/m^3, even a very low particle volumetric concentration (a few percent) results in a current density much greater than atmosphere. Such a range of particle volumetric concentration is easily reached in volcanic fountains (Dellino et al., 2014; Dufek, 2016).

It is to note that pyroclastic density currents are density stratified with a basal part much denser than the top, dilute, and turbulent part.

As long as there is a continuous feeding from the fountain, the mass flow rate is conserved, and the current is steady. This condition holds until the excess density is changed, along runout, as a result of air entrainment and particle sedimentation.

The entrainment of air from the surrounding atmosphere leads to a decrease of C, which results in a reduction of ρ_{mix}, which can be further reduced by particle sedimentation, with consequent flow deceleration. Eventually, when the excess density is nullified, the current stops flowing. At that point, if the fluid has a temperature still higher than the atmosphere, it could happen that the gas-particle mixture has a density lower than the surrounding, it becomes buoyant, and it forms a vertically directed phoenix cloud (Engwell et al., 2016; Neri & Macedonio, 1996).

Knowledge of the physical parameters that govern the rate of air entrainment in pyroclastic density currents is therefore of major importance for flow modeling and hazard assessment.

Specific models of the entrainment rate of pyroclastic density currents have not been developed until now, and empirical laws derived from hydraulics experiments are in use.

Morton et al. (1956), in a paper dealing with plume modeling, hypothesized that the rate of air entrainment from the surrounding, E, was a function of the plume ascent velocity. The entrainment is due to "stretching" and interpenetrating structures like the Kelvin-Helmoltz instabilities that enhance mixing at the flow interface. These structures develop as a function of fluid turbulence, and the entrainment rate is a time-averaged quantity. Such a hypothesis is maintained by Turner (1986) for gravity density currents moving down a slope. The entrainment coefficient is given by

$$E = \frac{U_{cross}}{U_{stream}} \tag{2}$$

where U_{cross} and U_{stream} are the current cross-stream and the stream average velocities, respectively.

In density currents the entrainment rate can change along runout as a function of the overall Richardson number Ri_0, which represents a ratio between buoyancy and inertial forces due to shear.

$$Ri_0 = \frac{g' H \cos\theta}{U^2} \tag{3}$$

with $g' = \frac{\rho_{mix} - \rho_{atm}}{\rho_{atm}}$ the reduced gravity, ρ_{atm} density of the atmosphere surrounding the current, θ the slope angle, and H current depth. The Richardson number is a measure of flow stratification stability, where shear favors the formation of flow instability structures and gravity tends to suppress them. The higher the Richardson number, the more the flow is stably stratified. The lower the Richardson number, the more flow instabilities grow and enhance entrainment.

We note that the definition of g' in equation (3) uses the conventional reduced gravity and not the alternative form of the reduced gravity, $g' = \frac{\rho_{mix} - \rho_{atm}}{\rho_{mix}}$, which has been proposed by some authors for pyroclastic density currents (e.g., Bursik & Woods, 1996). Turner (1986), basing on experiments made by Ellison and Turner (1959), proposed an equation of the entrainment coefficient as a function of the overall Richardson number, which has the form

$$E = \frac{0.08 - 0.1 Ri_0}{1 + 5 Ri_0} \tag{4}$$

Beghin et al. (1981) found that the entrainment rate was strongly dependent on the slope, and for angles higher than 5° the spatial growth rate of a finite volume cloud moving downslope has a linear dependence on the slope angle.

Hallworth et al. (1996) demonstrated, through experiments on Boussinesq gravity currents, that effective entrainment starts after a slumping phase whose position, along runout, depends on the aspect ratio of the current issuing from a lock gate. After the slumping phase, a similarity solution is attained in which velocity is scaled as a Froude number $Fr = U/(g' H)^{1/2}$. According to Hupperth and Simpson (1980), the value of the Froude number is set to $Fr = 1.19$.

Hopfinger and Tochon-Danguy (1977), by means of experiments in water tanks of finite volume clouds moving on a slope, found that

$$\frac{dH}{dx} = 3x10^{-3}(5+\alpha) \tag{5}$$

with α slope angle. In the experiments, flow velocity was in the range of 0.1 m/s and depth 0.1 m.

Parker et al. (1987) conducted experiments to determine the behavior of turbidity currents and produced steady flows seeded with silt particles in an inclined water tank. They added, to the results of their experiments, data from similar experiments carried out by Ellison and Turner (1959), Lofquist (1960), and Fukuoka and Fukushima (1980) and found an approximating function of the form

$$E_w = \frac{0.075}{(1+718R_i^{2.4})^{0.5}} \tag{6}$$

with E_w water entrainment and R_i the Richardson number that, with respect to the overall Richardson number Ri_0 does not account for the slope angle. Even in this case, flow velocity is about of 0.1 m/s and depth 0.1 m. The experiments from which equations (4)–(6) were derived relied on the Boussinesq approximation, which states that when the excess density between the current and the surrounding fluid is very small, it can be neglected in the equations of motion, except in the buoyancy terms. This approximation holds for aqueous fluids with a small particle volumetric concentration, like turbidity currents, but not for pyroclastic density currents or other gas-particle flows. In fact, if there is a 0.01 particle volumetric concentration in water (representing turbidity currents), an excess density with respect to the surrounding free water of the order of 1% is obtained, which can be considered negligible. The same particle concentration in gas implies an excess density of the order of 1,000% with respect to the surrounding atmosphere, which is clearly not negligible.

In volcanology, when entrainment is explicitly treated in the modeling of pyroclastic density currents, equations derived from experiments on aqueous flows of the type of turbiditic currents have been used, with a recommendation of caution in utilizing such laws for flows that have different scales, as it is the case of the Bursik and Woods (1996) model, in which equation (6) has been employed. Andrews (2014) and Breard and Lube (2017) found, by experiments, that the entrainment rate of pyroclastic density currents is highly variable, in dependence of the flow conditions and of the structure of the current (different values were found at the head and in the flow body). In particular, Breard and Lube (2017) report of a strong particle stratification in the current with a basal, concentrated part, characterized by a lower entrainment rate and an upper, dilute, and more turbulent part, with a higher entrainment rate, up to 0.22. Benage et al. (2016), by means of numerical simulations, confirm the current stratification found by Breard and Lube (2017) and report that the dilute part has entrainment coefficients 2–3 times larger than the basal bedload.

Recent research has shed new light on the behavior of snow avalanches, which are characterized by mixture density, flow velocity, and depth in the same ranges of pyroclastic density currents (Ancey, 2004; Turnbull et al., 2007). Differently from the small experimental aqueous currents of models (4)–(6), in both snow avalanches and pyroclastic density currents the regime is non-Boussinesq, and the inertia due to the large excess density cannot be neglected in the equations of motion. Ancey (2004), for a finite volume snow avalanche cloud moving on a slope, uses the equation for volume variation $\frac{dV}{dt} = \alpha_v\sqrt{V}U$, with V being the volume per unit width and α_v volume growth rate, the latter being analogous to the entrainment rate E of constant flux currents. Basing on experiments and unpublished data by Beghin et al. (1981) and data from Fernando (1991), Ancey (2004) proposes a relationship between the volumetric growth rate and the overall Richardson number, based on a two-piece function, of the form $\alpha_v = e^{-1.6Ri_0^2}$ for $Ri_0 \leq 1$ and $\alpha_v = 0.2/Ri_0$ for $Ri_0 > 1$. The experiments cover a small range of Ri_0, between 0.23 and 1.32, and caution is recommended when using the relationship for the whole range of natural events.

Unfortunately, laboratory experiments on strong non-Boussinesq flows are very rare. According to Étienne et al. (2006) only lock-exchange flow experiments using gas allow reaching very high density ratios and say: "... it is hardly feasible to use gases for gravity current or dense cloud experiments on slopes because of the large gas volumes needed ... ."

In order to cover this gap, in the present research, non-Boussinesq gas-particle gravity currents simulating pyroclastic density currents were produced by experiments.

Figure 1. Display mount of experiments. (a) The two racks of gas bottles. (b) A hub of solenoid valves connecting the long to short hoses. (c) The 3.2-m cylindrical conduit. (d) Formation of the dense gas-particle fountain. On the right, the two mock-ups representing morphological obstacles are shown by the arrow. (e) Collapse of the fountain on the ground and generation of the density current. (f) General view of the thin layer of deposit.

2. Experiments

2.1. Setup, materials, and methods

The purpose of experiments was to obtain measurable gas-particle flows, scalable to natural pyroclastic density currents, by which to develop a model of air entrainment. Density currents were generated by the impingement on the ground of a gas-particle fountain issuing from a cylindrical conduit. The experiments were performed with the apparatus described in detail by Dellino et al. (2007, Dellino, Dioguardi, et al., 2010, Dellino, Büttner, et al., 2010, 2014).

The gas source of the experiments consisted of two racks of 16 bottles (Figure 1a) of compressed gas (50 L each at 200 bars). Nitrogen was used in order to avoid oxidation of the metallic parts.

The gas bottles were in line with manometers and were connected, via two valves and two hubs, to 18 steel-reinforced rubber hoses each 30 m long with 8-mm internal diameter. Two hubs of high-speed solenoid valves, where the driving pressure was monitored by a transducer, connected the 18 long hoses to 18 short hoses of 1.5-m length, 8-mm internal diameter (Figure 1b). The short hoses were connected to 18 blow nozzles in the base plate of a 3.2-m-high conduit with an internal diameter of 0.6 m (Figure 1c), which was loaded with up to 360 kg of particulate material. Particles were collected from the pyroclastic deposits of Vesuvius and Campi Flegrei volcanoes in Southern Italy. The coarser composition (from Vesuvius) ranged from a few micrometres to a few centimetres, with a median size $D = 0.75$ mm, while the finer one (from

Campi Flegrei) was made mostly of fine ash, with a median size $D = 0.066$ mm (see the grain-size distributions in the Figure S1 in the supporting information).

The particle load, gas pressure, and grain size of the particulate material were varied among runs as to obtain flows of different speed, particle concentration, and granulometry.

On previous papers (Dellino et al., 2011; Dellino et al., 2014) experiments carried out both at ambient temperature and up to 300 °C demonstrated that, in the case of collapsing fountains (in contrast with convective plumes), temperature does not play a major role neither in determining the jet dynamics nor in the sedimentation from the base of the ground-moving density current. The effect of temperature is just that of modifying the density stratification of the current. The same effect can be obtained by varying the particle volumetric concentration of the gas-particle mixtures, which is the choice of the present paper, where experiments were carried out at ambient temperature.

The experiments were monitored with a network of high-definition video cameras (recording at 50 frames per second) that allowed measurements of the geometry (including heights, lengths, and volume) and fountain speed, and speed and geometry of the density currents. The slope on the ground was 9° in the first 8 m of radial distance from the conduit base and dropped to zero at longer distance. At a radial distance of 5 m from the conduit, two mock-ups (simulating morphologic obstacles) of 1-m length and 0.3-m height were placed on the ground (Figure 1d) as for analyzing the effect of a topographic barrier on the flow.

The experiment started by opening the valves that connected the gas source to the long hoses. By means of manometers, the pressure of the gas in the long hoses was regulated. When the valves were closed, a volume of 28 L of compressed gas at the desired pressure was loaded into the long hoses. Upon opening the solenoid valves, the gas charge rapidly passed through the short hoses and eventually was injected into the particulate material through the blow nozzles of the base plate. The so formed two-phase flow started moving as a granular mass that expanded while it was accelerated along the conduit. The gas-particle mixture was finally expelled out of the conduit, adjusted in pressure with respect to the surrounding atmosphere (Dellino et al., 2014), in the form of a dense fountain, with an exit velocity, U_0, up to 17.5 m/s.

The flow alimentation at conduit exit was assumed as steady during the experiment, since the gas flow rate entering the conduit, as recorded by a high-precision, high-frequency pressure transducer, resulted to be constant over the time scale of the experiment. The particulate mass flow rate PFR_0 at conduit exit was calculated by the ratio of the total mass of particles and the duration of flow alimentation.

The gas-particle mixture density at conduit exit was calculated, assuming that gas and particle velocities were fully coupled, as

$$\rho_0 = \frac{PFR_0}{\pi R_0^2 U_0} \tag{7}$$

where R_0 is the internal conduit radius.

The total mass flow rate at conduit exit, MFR_0, was calculated as

$$MFR_0 = U_0 \rho_0 \pi R_0^2 \tag{8}$$

The fountain reached a maximum height Z (over 14 m in the case of Figure 3d), which followed the prescription of Bernoulli's equation of conservation of total pressure $Z = {U_0}^2/2g$ (Dellino et al., 2014). It means that the density of the gas-particle mixture and mass flow rate did not change along the ascending-descending trajectory:

$$MFR_0 = MFR_{\text{imp}} \tag{9}$$

where the right-hand side is the mass flow rate of the fountain impinging on the ground, with impact velocity normalized, with respect to conduit exit velocity, to the extra height between the conduit length and the ground (which is 3.2 m).

The particle load of experiments ranged between 180 and 360 kg. Experiment parameters at conduit exit are reported in Table S1. In particular, the Reynolds number was in the order of 10^7, meaning that fully

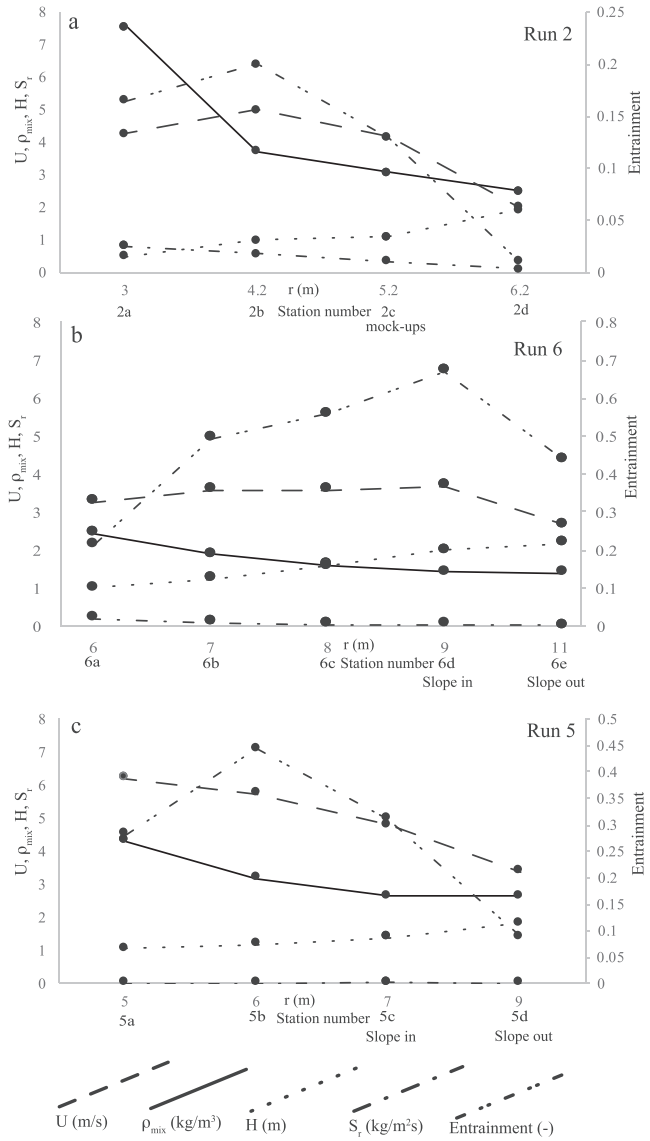

Figure 2. Variation of experiments parameters along runout. (a) Run 2 of Table S1. (b) Run 6 of Table S1. (c) Run 5 of Table S1. On the horizontal axis, the distance from the fountain impact and the station number, as they are reported in the data set of Table S1, are shown. The vertical axis on the left refers to U (current velocity), ρ_{mix} (current density), and H (current depth). The right axis refers to the E (entrainment coefficient).

turbulent flows were reached at conduit exit. These conditions ensure that the experiments were dynamically similar to actual eruption columns (Dellino et al., 2014). Upon hitting the ground (Figure 1e), the fountain resembled the collapse of an eruptive column similar to that generating a natural pyroclastic density current.

After the impact of the fountain on the ground, the normal stress of the fluid was transformed into a tangential stress, leading to a shear flow that evolved laterally into a few-meters-thick, fully turbulent gas-particle current, moving at several meters per second. It spread radially for more than 20 m and left on the ground a thin bed representing sedimentation from the current (Figure 1f).

In this paper, six runs are considered. For each run, data of the entrainment rate E, the overall Richardson number Ri_0, and the sedimentation rate S_r of the density currents were collected at multiple stations, along flow runout. A data set of 20 measurements was obtained, which is shown in Table S1.

As to ensure that data were collected from sustained flows, measurements were made along runout as long as the fountain was continuously feeding the current. The entrainment rate was calculated, at each station, using the axisymmetric formulation of the volume conservation:

$$EU = \frac{dUHr}{rdr} \tag{10}$$

where r is the radial distance of the station from the fountain impact on the ground and U is the velocity at the station.

$dUHr$ was calculated as $UHr - U_{up}H_{up}r_{up}$, and rdr as $r(r - r_{up})$ where U, h, and r are the velocity, depth, and distance values at the station and U_{up}, H_{up}, and r_{up} are the velocity, depth, and distance values at an upstream location. The distance between the station and the upstream location ranged between 1 and 3 m.

The change of volume due to particle sedimentation was assumed as not significant.

Ri_0 was calculated by means of equation (3), and the sedimentation rate S_r was estimated as the mass sedimented per unit area, over the time of sedimentation, which was measured by the time elapsed between the arrival of the current and the end of the fountain feeding the current (Dellino et al., 2019). The mass of sediment per unit area was calculated by sampling the sediment over a rectangle of known area and weighting it.

At each station, current velocity and depth were measured at flow front as the average value of five successive video frames, with the third frame centered around the location. Depth and velocity values, which were used in equation (10) for the calculation of the entrainment rate, are, therefore, averaged over a time interval of 0.1 s. This means that the entrainment rate represents the macroscopic time-averaged behavior of the current, as it is in the case of other experimental measurements as those of Parker et al. (1987). Our measurements do not take into consideration oscillations around very small time scales and lengths, which are due to the fluctuating nature of the Kelvin-Helmoltz instabilities at the mixing interface of turbulent currents that are captured by instantaneous measurements (see Breard & Lube, 2017).

The mass flow rate of the current, MFR, was calculated, at each station, by subtracting the mass of sediment deposited at previous stations from the mass flow rate at the impact, MFR_{imp}, and using as the cross-sectional area of the flow, the value measured at each station by multiplying H for $2\pi r$, where r is the radial distance, from the impact, reached by the flow front. The current density at each station was calculated by $\rho_{mix} = \frac{MFR}{UH2\pi r}$.

2.2. Results

The fluid-flow parameters recorded in the experiments (see Table S1) are in the same order of magnitude of natural pyroclastic density currents (see Table S2), meaning that a scaling between experiments and nature can be proposed. The current velocity was up to 11.9 m/s; the Reynolds number $Re = \frac{\rho_f u H_T}{\mu}$, with μ fluid viscosity, was always in excess of 10^5, meaning the flow was fully turbulent. The overall Richardson number ranged between 0.25 and 5.95, and the entrainment coefficient ranged between 0.01 and 0.67. The density of the gas-particle mixture ranged between 1.5 and 12.8 kg/m^3.

The analysis of runs where the current was measured at a sufficient number of stations allows visualizing the change of current parameters as a function of radial distance. In run 2 (Figure 2a), a strong acceleration occurs in the vicinity of the impact against the ground and leads to a rapid decrease of the overall Richardson number and an increase of the entrainment rate between stations 2a and 2b. After the acceleration phase, a rapid deceleration occurs, accompanied by a high sedimentation rate that causes a rapid decrease of current density. In this run, measurements were made along the direction where the flow intercepted the mock-ups. At the encounter between the flow and the mock-ups, which happened between stations 2d and 2e, a further strong deceleration, a rapid increase of depth, a rapid increase of the overall Richardson number, and a sharp decrease of the entrainment rate occurred.

In run 6 (Figure 2b), at the radial distance where the slope goes to zero, a strong deceleration occurs that leads to a rapid increase of current depth, and a rapid increase of the overall Richardson number and a decrease of the entrainment rate between station 6d where the slope change starts (slope in of Figure 2b) and station 6e where the slope goes to zero (slope out of Figure 2b).

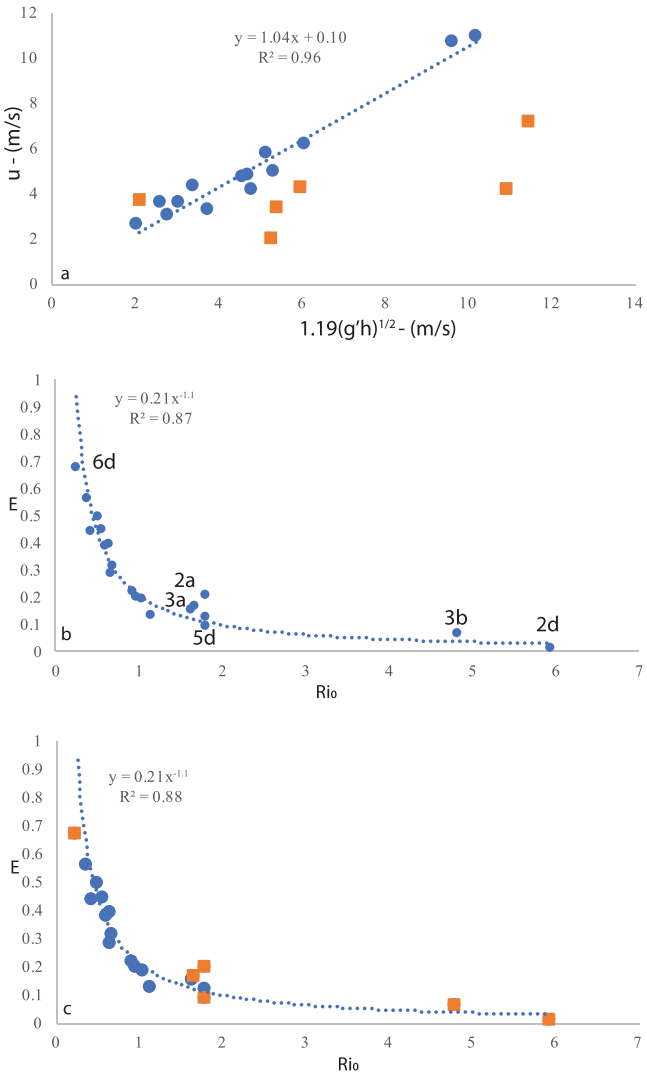

Figure 3. Models. (a) Similarity diagram. Circles represent data points of stations without strong velocity changes. Squares represent data points of stations with strong velocity changes. The equation of the regression line, which is relative only to circles, and the correlation coefficient are inset. (b) The power law model of E as a function of Ri_0. The regression line and the correlation coefficient are also inset. The stations with strong velocity changes are lettered according to Table S1. (c) The power law model of E as a function of Ri_0 calculated without the stations with strong changes of velocity. The circles represent the stations without strong velocity changes; the squares represent stations with strong changes of velocity. The regression line equation is calculated without stations with strong changes of velocity. The correlation coefficient is also inset.

Runs 2 and 6 were fed with the particulate material of the coarse size, while run 5 was fed with the fine ash composition. In run 5 (Figure 2c), the trend of velocity as a function of radial distance is affected by less abrupt changes with respect to the other runs, likely due to the much smaller sedimentation rate, determined by the lower settling rate of fine-ash particles. A small "kink" in the trend is visible as the current approaches the slope change at higher radial distance (station 5c), causing a deceleration, a depth increase, an increase of the overall Richardson number, and a decrease of the entrainment rate between stations 5c (slope in of Figure 2c) and 5d (slope out of Figure 2c).

Run 3 demonstrates the rapid change of the entrainment rate of a strongly decelerating run (stations 3a and 3b of Table S1).

As for assessing whether similarity was attained in the currents, the whole data set was plotted against the solution adopted by Hupperth and Simpson (1980), $U = 1.19(g'H)^{1/2}$, as shown in Figure 3a. Only the points

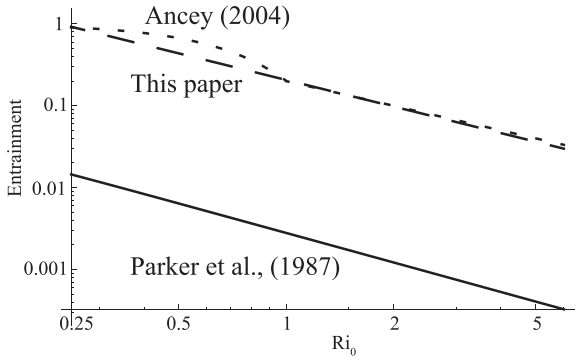

Figure 4. Diagram showing log-log plots of the entrainment rate models as a function of the overall Richardson number of Parker et al. (1987), solid line; Ancey (2004), dotted line; and this paper, dashed line.

relative to strong velocity changes (squares) caused by (i) the fountain impact (stations 2a, 3a, and 3b of Table S1); (ii) the occurrence of an obstacle (station 2d of Table S1); and (iii) a slope change (stations 5d and 6d of Table S1) show a marked scatter. For all other stations, where less strong changes of velocity affected the current, the regression line, which was obtained by the least squares method, can be approximated, with a small error, to the form $y = x$, with a good correlation coefficient. This means that a similarity solution was obtained by the experimental currents. The Richardson number was calculated using the original formulation of the reduced gravity g' (see previous section), differently from what has been done in other models of pyroclastic density currents (e.g., Bursik & Woods, 1996); we suggest, therefore, that this is the correct formulation of g' that leads to a similarity solution.

In Figure 3b, a diagram of the entrainment rate as a function of the overall Richardson number is shown. A power law with equation

$$E = 0.21 {Ri_0}^{-1.1} \tag{11}$$

which was obtained by the statistical least squares method, fits well the whole data set, with a good correlation coefficient. A small scatter is visible, which is related to the data points of stations characterized by strong velocity changes. It is to note that the data points related to strong changes of velocity are much closer to the fitting line when compared to the larger scatter that the same stations show on the diagram of the similarity solution of Figure 3a. The equation of the fitting line is identical with and without the data points of the stations with strong velocity changes, as it is evidenced by a comparison with Figure 3c, where the stations with strong changes of velocity are marked by squares, and the increase of the correlation coefficient without the data points of the stations with strong velocity changes is not statistically significant. This outcome makes equation (11) usable also in the case of currents that respond to perturbations of the flow rate, or to changes in slope, or to the occurrence of morphological obstacles, which are likely conditions in large-scale ground-hugging geophysical mass flows, as pyroclastic density currents. In Figure 4 a comparison between the law of equation (11) proposed in this paper; the model of equation (6), which was proposed by Parker et al. (1987) for aqueous currents and was used by Bursik and Woods (1996) for modeling pyroclastic density currents; and the model proposed by Ancey (2004) for snow avalanches, is shown. The model of Parker et al. (1987) always has a much lower entrainment than equation (11), in the whole range of Richardson number. This is probably due to the different scales of instabilities at the mixing interface, which are much larger in highly turbulent gas-particle mixtures compared to those in less turbulent aqueous currents. The Reynolds number of our experiments (see Table S1) is, in fact, at least 3 orders of magnitude higher than the one obtained by previous experiments on aqueous flows by Turner (1986), Hopfinger and Tochon-Danguy (1977), and Parker et al. (1987).

By the inspection of Figure 4 it is also noted that equation (11) is strikingly similar to that proposed by Ancey (2004) in the range of Ri_0 higher than 1. In fact, our model, can be conveniently simplified as $E = 0.2/Ri_0$. The little difference between the model of this paper and the two-piece function of Ancey (2004), which is noted at Ri_0~0.5, vanishes at lower Ri_0values; thus, it does not affect much the general similarity of the two models. This small difference is probably not related to a real physical effect but, more likely, to data processing or interpolation. In fact, by inspecting Figure 2 of Ancey (2004) it is noted that the two-piece function is constructed by means of a few data points and that the use of a single line with equation $E = 0.2/Ri_0$ would not introduce much of a variance with respect to the two-piece function. The strong similarity of pyroclastic density currents and snow avalanches, which was already suggested by Turnbull et al. (2007) and Ancey (2004) is, indeed, confirmed by the model of the present paper.

3. Discussion and Conclusion

The large-scale experiments allowed the development of a model that is similar to the law proposed by Ancey (2004) for snow avalanches and is verified in the range of overall Richardson number between 0.25 and 5.95, which is a much wider range compared to that resulting from previous experiments on small

aqueous Boussinesq flows. The entrainment rate rapidly readjusts to flow perturbations, making the model applicable also in the case of flows with rapid changes of velocity. By means of the experiments it was demonstrated that sharp changes are caused by flow perturbations that occur (i) at the impact of the fountain, which causes an acceleration of the current, with an increase of the entrainment rate; (ii) at the break in slope that causes a strong deceleration with an increase of flow depth and a decrease of air entrainment; and (iii) in the presence of topographic obstacles that lead to a deceleration and decrease of air entrainment.

Such changes can strongly influence the behavior of pyroclastic density currents. Sharp changes of velocity and excess density, which frequently occur over the flow dispersal area, especially in zones of abrupt morphological "jumps," lead to strong variations of current dynamic pressure and particle volumetric concentration, which are the main source of hazard of pyroclastic density currents (Dellino et al., 2008, 2011; Mele et al., 2015; Valentine, 1998). Similar effects can be expected in the case of snow avalanches, which share many characteristics with pyroclastic density currents (Ancey, 2004; Turnbull et al., 2007). The presence of a significant amount of fine ash tends, instead, to prevent the rapid changes of excess density due to sedimentation (Dellino et al., 2019) and allows to maintain a larger mobility of the current (Dellino et al., 2019).

As for fully accounting the effect of air entrainment on flow mobility, the use of models as the one proposed in this paper is therefore recommended when modeling hazardous geophysical mass flows as pyroclastic density currents and snow avalanches.

Acknowledgments
Bernd Zimanowski and Ralf Büttner shared with the authors the experiment design and development. They are gratefully thanked. The paper greatly benefited from the revision of Gert Lube and Kristen Fauria. Published with permission of the Executive Director of British Geological Survey (UKRI). Data can be found at the Zenodo repository with the following link https://zenodo.org/search?page=1&size=20&q=dellino, with DOI 10.5281/zenodo.3408690.

References

Ancey, C. (2004). Powder-snow avalanches: Approximation as non-Boussinesq clouds with a Richardson number-dependent entrainment function. *Journal of Geophysical Research*, *109*, F01005. https://doi.org/10.1029/2003JF000052

Andrews, B. J. (2014). Dispersal and air entrainment in unconfined dilute pyroclastic desnity currents. *Bulletin of Volcanology*, *76*, 1–14.

Beghin, P., Hopfinger, E. J., & Britter, R. E. (1981). Gravitational convection from instantaneous sources on inclined boundaries. *Journal of Fluid Mechanics*, *107*, 407–422. https://doi.org/10.1017/S0022112081001821

Benage, M. C., Dufek, J., & Mothes, P. A. (2016). Quantifying entrainment in pyroclastic density currents from the Tunguarahua eruption, Ecuador: integrating field proxies with numerical simulations. *Geophysical Research Letters*, *43*, 6932–6941. https://doi.org/10.1002/2016GL069527

Breard, E. C. P., & Lube, G. (2017). Inside pyroclastic density currents—Uncovering the enigmatic flow structure and transport behavior in large-scale experiments. *Earth and Planetary Science Letters*, *458*, 22–36.

Bursik, M. I., & Woods, A. W. (1996). The dynamics and thermodynamics of large ash flows. *Bulletin of Volcanology*, *58*(2-3), 175–193.

Dellino, P., Büttner, R., Dioguardi, F., Doronzo, D. M., La Volpe, L., Mele, D., et al. (2010). Experimental evidence links volcanic particle characteristics to pyroclastic flow hazard. *Earth and Planetary Science Letters*, *295*, 314–320.

Dellino, P., De Astis, G., La Volpe, L., Mele, D., & Sulpizio, R. (2011). Quantitative hazard assessment of phreatomagmatic eruptions at Vulcano (Aeolian Islands, Southern Italy) as obtained by combining stratigraphy, event statistics and physical modelling. *Journal of Volcanology and Geothermal Research*, *201*(1-4), 364–384.

Dellino, P., Dioguardi, F., Doronzo, D. M., & Mele, D. (2019). The rate of sedimentation from turbulent suspension: An experimental model with application to pyroclastic density currents and discussion on the grain-size dependence of flow runout. *Sedimentology*, *66*(1), 129–145.

Dellino, P., Dioguardi, F., Mele, D., D'Addabbo, M., Zimanowski, B., Büttner, R., et al. (2014). Volcanic jets, plumes, and collapsing fountains: evidence from large-scale experiments, with particular emphasis on the entrainment rate. *Bulletin of Volcanology*, *76*, 834.

Dellino, P., Dioguardi, F., Zimanowski, B., Büttner, R., Mele, D., La Volpe, L., et al. (2010). Conduit flow experiments help constraining the regime of explosive eruptions. *Journal of Geophysical Research*, *115*, B04204. https://doi.org/10.1029/2009JB006781

Dellino, P., Mele, D., Sulpizio, R., La Volpe, L., & Braia, G. (2008). A method for the calculation of the impact parameters of dilute pyroclastic density currents based on deposits particle characteristics. *Journal of Geophysical Research*, *113*, B07206. https://doi.org/10.1029/2007JB005365

Dellino, P., Zimanowski, B., Büttner, R., La Volpe, L., Mele, D., & Sulpizio, R. (2007). Large-scale experiments on the mechanics of pyroclastic flows: Design, engineering, and first results. *Journal of Geophysical Research*, *112*, B04202. https://doi.org/10.1029/2006JB004313

Dufek, J. (2016). The fluid mechanics of pyroclastic density currents. *Annual Review of Fluid Mechanics*, *48*, 459–485.

Ellison, T., & Turner, J. (1959). Turbulent entrainment in stratified flows. *Journal of Fluid Mechanics*, *6*, 423–448.

Engwell, S., de' Michieli Vitturi, M., Esposti Ongaro, T., & Neri, A. (2016). Insights into the formation and dynamics of coignimbrite plumes from one-dimensional models. *Journal of Geophysical Research: Solid Earth*, *121*, 4211–4231. https://doi.org/10.1002/2016JB012793

Étienne, J., Rastello, M., & Hopfinger, E. J. (2006). Modelling and simulation of powder-snow avalanches. *Comptes Rendus Mécanique*, *334*(8-9), 545–554.

Fernando, H. J. S. (1991). Turbulent mixing in stratified fluids. *Annual Review of Fluid Mechanics*, *23*, 455–493.

Fukuoka, S., & Fukushima, Y. (1980). Mechanics of gravity currents advancing into stratified reservoir. *Proceedings. Japan Society of Civil Engineers*, *293*, 65–77.

Hallworth, M. A., Huppert, H. E., Phillips, J. C., & Sparks, R. S. J. (1996). Entrainment into two-dimensional and axisymmetric turbulent gravity currents. *Journal of Fluid Mechanics*, *308*, 289–311.

Hopfinger, E. J., & Tochon-Danguy, J. C. (1977). A model study of powder-snow avalanches. *Journal of Glaciology*, *81*, 343–356.

Hupperth, E., & Simpson, J. E. (1980). The slumping of gravity currents. *Journal of Fluid Mechanics*, *99*(7), 85–799.

Lofquist, K. (1960). Flow and stress near an interface between stratified liquids. *Physics of Fluids*, *3*(2), 158–175. https://doi.org/10.1063/1.1706013

Mele, D., Dioguardi, F., Dellino, P., Isaia, R., Sulpizio, R., & Braia, G. (2015). Hazard of pyroclastic density currents at the Campi Flegrei Caldera (Southern Italy) as deduced from the combined use of facies architecture, physical modeling and statistics of the impact parameters. *Journal of Volcanology and Geothermal Research*, *299*, 35–53.

Morton, B. R., Taylor, G. I., & Turner, J. S. (1956). Turbulent gravitational convection from maintained and instantaneous sources. *Proceeding of the Royal Society A*, *234*, 1–23.

Neri, A., & Macedonio, G. (1996). Numerical simulation of collapsing volcanic columns with particles of two sizes. *Journal of Geophysical Research*, *101*(4), 8153–8174.

Parker, G., Garcia, M., Fukushima, Y., & Yu, W. (1987). Experiments on turbidity currents over an erodible bed. *Journal of Hydraulic Research*, *25*(1), 123–147. https://doi.org/10.1080/00221688709499292

Sulpizio, R., Dellino, P., Doronzo, D. M., & Sarocchi, D. (2014). Pyroclastic density currents: state of the art and perspectives. *Journal of Volcanology and Geothermal Research*, *283*, 36–65.

Turnbull, B., McElwaine, J. N., & Ancey, C. (2007). Kulikovskiy-Sveshnikova-Beghin model of power snow avalanches: Development and application. *Journal of Geophysical Research*, *112*, F01004. https://doi.org/10.1029/2006JF000489

Turner, J. S. (1986). Turbulent entrainment: The development of the entrainment assumption, and its application to geophysical flows. *Journal of Fluid Mechanics*, *173*, 431–471.

Valentine, G. A. (1998). Damage to structures by pyroclastic flows and surges, inferred from nuclear weapons effects. *Journal of Volcanology and Geothermal Research*, *87*(1-4), 117–140.